

Full-gap superconductivity in non-centrosymmetric Re_6Zr , $\text{Re}_{27}\text{Zr}_5$ and $\text{Re}_{24}\text{Zr}_5$

K. Matano¹, R. Yatagai¹, S. Maeda¹, and Guo-qing Zheng^{1,2}

¹*Department of Physics, Okayama University, Okayama 700-8530, Japan*

²*Institute of Physics, Chinese Academy of Sciences,*

and Beijing National Laboratory for Condensed Matter Physics, Beijing 100190, China

(Dated: December 9, 2016)

Abstract

Non-centrosymmetric superconductor Re_6Zr has attracted much interest, for its possible unconventional superconducting state with time reversal symmetry broken. Here we report the $^{185/187}\text{Re}$ nuclear quadrupole resonance (NQR) measurements on Re_6Zr ($T_c = 6.72$ K) and the isostructural compounds $\text{Re}_{27}\text{Zr}_5$ ($T_c = 6.53$ K) and $\text{Re}_{24}\text{Zr}_5$ ($T_c = 5.00$ K). The nuclear spin-lattice relaxation rate $1/T_1$ shows a coherence peak below T_c and decreases exponentially at low temperatures in all three samples. The superconducting gap Δ derived from the $1/T_1$ data is $2\Delta = 3.58 k_B T_c$, $3.55 k_B T_c$, and $3.51 k_B T_c$ for Re_6Zr , $\text{Re}_{27}\text{Zr}_5$, and $\text{Re}_{24}\text{Zr}_5$, respectively, which is close to the value of $3.53 k_B T_c$ expected for weak-coupling superconductivity. These data suggest conventional s -wave superconductivity with a fully-opened gap in this series of compounds.

I. INTRODUCTION

Superconductors with broken symmetries, such as broken time-reversal symmetry¹ or broken spin-rotation symmetry², have attracted great attention. In particular, the role of crystal structure in the emergence of unconventional superconducting states has been studied extensively in recent years.

In superconductors with an inversion center in the crystal structure, either an even-parity spin-singlet or an odd-parity spin-triplet superconducting state is realized. However, in non-centrosymmetric superconductors, a parity-mixed superconducting state is allowed and an antisymmetric spin-orbit coupling (ASOC) interaction is induced³⁻⁵. The parity-mixing extent is determined by the strength of the ASOC.

Indeed, some non-centrosymmetric superconductors show novel features. For example, the isostructural $\text{Li}_2\text{Pd}_3\text{B}$ and $\text{Li}_2\text{Pt}_3\text{B}$ show contrasting behaviors. $\text{Li}_2\text{Pd}_3\text{B}$ exhibits conventional BCS-type properties⁶, while $\text{Li}_2\text{Pt}_3\text{B}$ is a spin-triplet dominant superconductor⁷ with nodes in the gap function^{7,8}. In this case, a different ASOC due to the difference of peculiar crystal structure distortion and atomic number were responsible for the different superconducting states⁹. After the discovery of spin-triplet superconductivity in $\text{Li}_2\text{Pt}_3\text{B}$, extensive studies have been performed to search for novel superconductivity in non-centrosymmetric superconductors containing heavy elements such as $\text{Mg}_{10+x}\text{Ir}_{19-y}\text{B}^{10}$, BiPd^{11} , and ScIrP^{12} , but parity-mixing is found to be weak^{13,14}, due to the crystal structure that does not lead to strong ASOC enhancement.

Recently, more novel properties were reported in some non-centrosymmetric superconductors. For example, a small internal magnetic field was detected below T_c in non-centrosymmetric LaNiC_2 , which was interpreted as due to a breaking of time reversal symmetry in the superconducting state¹, although a relation between the breaking of inversion symmetry and time reversal symmetry is unclear.

Non-centrosymmetric Re_6Zr is a new candidate of time reversal symmetry-breaking superconductor. Re_6Zr has an α -Mn type cubic crystal structure with space group $I\bar{4}3m^{15}$ and a large upper critical field close to Pauli limit¹⁶. Figure 1 shows the α -Mn type crystal structure, which has four independent crystallographic sites Mn I : $2a$ (Wyckoff), $\bar{4}3m$ (Hermann-Mauguin), Mn II : $8c$, $3m$, Mn III : $24g_1$, m , and Mn IV : $24g_2$, m^{17} . Among them, only the Mn I ($2a$, $\bar{4}3m$) site has an inversion center. An internal magnetic field was detected

in the superconducting state by muon spin relaxation or rotation (μ SR) measurements¹⁶. The result was ascribed to broken time reversal symmetry in the superconducting state. It is known that a chiral p -wave state or a chiral d -wave state can produce a tiny internal magnetic field^{18,19}.

In order to investigate the gap structure, we performed the nuclear quadrupole resonance (NQR) measurements on Re_6Zr , and the iso-structural compounds $\text{Re}_{27}\text{Zr}_5$ and $\text{Re}_{24}\text{Zr}_5$. These compounds have an α -Mn type crystal structure but with different superconducting transition temperatures, with $\text{Re}_{24}\text{Zr}_5$ being stoichiometric. The NQR measurement performed at zero magnetic field is one of the most powerful methods for the study of the superconducting gap symmetry. We find that all the three compounds show the superconducting properties consistent with a conventional BCS gap symmetry.

II. EXPERIMENTAL

The polycrystalline samples of Re_6Zr , $\text{Re}_{27}\text{Zr}_5$, and $\text{Re}_{24}\text{Zr}_5$ in this study were synthesized by the arc-melting method. The Re (99.99%) and Zr (99.9%) were arc-melted under an argon atmosphere. The difference of mass before and after the melting was less than 1% for all samples. The melted ingots were crushed into powders for X-Ray diffraction (XRD) and NQR measurements. The $\text{Cu K}\alpha$ radiation is used for the XRD measurements. The T_c was determined by measuring the ac susceptibility using the *in situ* NQR coil. A standard phase-coherent pulsed NMR spectrometer was used to collect data. The nuclear spin-lattice relaxation rate was measured by using a single saturation pulse. The spin echo was observed with a sequence of $\pi/2$ pulse ($4\ \mu\text{s}$) - $30\ \mu\text{s}$ - π pulse ($8\ \mu\text{s}$).

III. RESULTS AND DISCUSSIONS

Figure 2 shows the XRD patterns and the ac susceptibility results for Re_6Zr , $\text{Re}_{27}\text{Zr}_5$ and $\text{Re}_{24}\text{Zr}_5$. The lattice constant a is $9.714\ \text{\AA}$ for Re_6Zr , which is a little shorter than the reported value $9.698\ \text{\AA}$ ¹⁵. The T_c for Re_6Zr is $6.72\ \text{K}$, which is very close to $6.75\ \text{K}$ reported in Ref.¹⁶. The obtained lattice constant and T_c are shown in Table 1. For Re_6Zr and $\text{Re}_{27}\text{Zr}_5$, the XRD patterns can be fitted by Rietveld method. For $\text{Re}_{24}\text{Zr}_5$, some unidentified peaks are observed. The line width increases with increasing Zr composition,

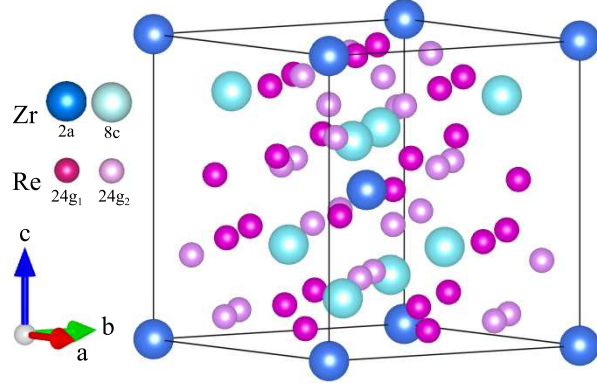


FIG. 1. (color online) Crystal structure of α -Mn type Re-Zr system. It is a cubic structure with space group $I43m$.

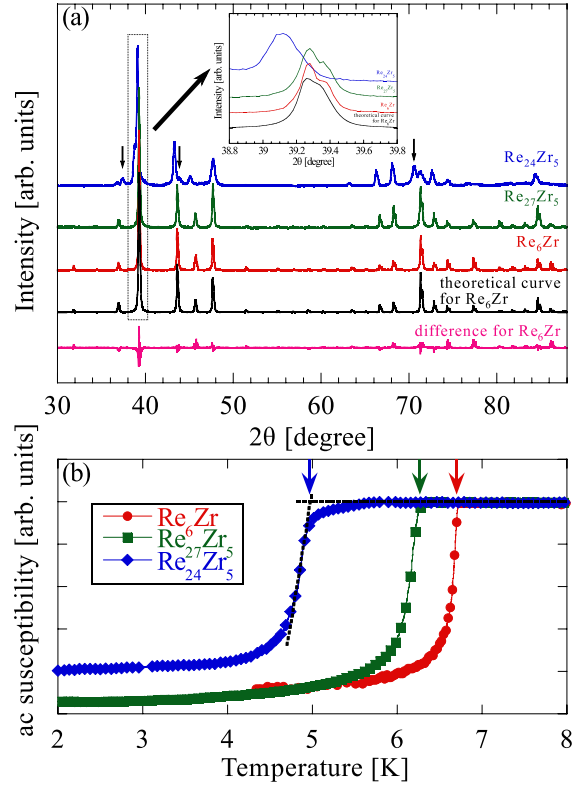


FIG. 2. (a) XRD patterns for Re_6Zr , $\text{Re}_{27}\text{Zr}_5$, and $\text{Re}_{24}\text{Zr}_5$. The theoretical curve and the difference between the theoretical curve and the observed XRD are obtained by the Rietveld method. Arrows indicate unidentified peaks. For clarity, in the inset we show the enlarged part in the range of 38.8 - 39.8 degrees. (b) Ac susceptibility measured using the *in situ* NQR coil at zero magnetic field. The arrows indicate T_c for each sample.

TABLE I. Crystal structure, the NQR parameters for ^{187}Re , and the superconductivity parameters for Re_6Zr , $\text{Re}_{27}\text{Zr}_5$, and $\text{Re}_{24}\text{Zr}_5$.

	Re_6Zr ($\text{Re}_{30}\text{Zr}_5$)		$\text{Re}_{27}\text{Zr}_5$		$\text{Re}_{24}\text{Zr}_5$	
lattice constant [\AA]	9.714		9.726		9.762	
2Δ [$k_B T_c$]	3.58		3.55		3.51	
T_c [K]	6.72		6.53		5.00	
site	A	B	A	B	A	B
ν_Q [MHz]	42	84	42	83	42	75
η	0.6	0.6	0.6	0.6	0.6	0.7
$FWHM$ ($\pm 1/2 \leftrightarrow \pm 3/2$) [MHz]	13	25	14	20	16	23
$FWHM$ ($\pm 3/2 \leftrightarrow \pm 5/2$) [MHz]	19	36	24	34	28	37

which suggests that impurities or crystal distortion increases with increasing Zr composition. In the ac susceptibility for $\text{Re}_{24}\text{Zr}_5$, a small shoulder can be seen around T_c , which is likely attributable to the sample inhomogeneity. Similar result has been reported in the Nb-Re systems²⁰. In α -Mn type systems, $\text{Re}_{24}\text{Zr}_5$ is stoichiometric, while Re_6Zr and $\text{Re}_{27}\text{Zr}_5$ are non-stoichiometric with Re-rich compositions. In the $\text{Re}_x\text{Zr}_{1-x}$ binary phase diagram²¹, a single phase α -Mn structure can be obtained only in a narrow range with $0.82 \leq x \leq 0.87$. The Re-to-Zr ratio is 82.8 : 17.2 for the stoichiometric $\text{Re}_{24}\text{Zr}_5$, which is quite close to the limit to obtain a single phase. On the other hand, the Re-to-Zr ratio is 84.4 : 15.6 for $\text{Re}_{27}\text{Zr}_5$ and 85.7 : 14.3 for Re_6Zr . As seen in Fig. 2, the stoichiometric $\text{Re}_{24}\text{Zr}_5$ compound showed a small amount of additional peaks in the XRD chart, which is likely due to the fact that the $\text{Re}_{24}\text{Zr}_5$ is close to the phase boundary.

Figure 3 shows the $^{185/187}\text{Re}$ -NQR spectra at $T = 10$ K for the three samples. Four peaks were observed for all samples. The Re nuclei have a spin $I = \frac{5}{2}$, which will result in two NMR transitions. In the Re-Zr systems with α -Mn type structure, the unit cell has 58 atoms that are distributed into two Zr sites ($2a$, $8c$) and two Re sites ($24g_1$, $24g_2$)²². Furthermore, Re has two isotopes ^{185}Re (natural abundance 37.5%) and ^{187}Re (62.5%). As a result, eight peaks for this compound are expected in principle. However, the difference in the nuclear quadrupole moment Q of ^{185}Re ($2.7 \times 10^{-24} \text{ cm}^2$) and ^{187}Re ($2.6 \times 10^{-24} \text{ cm}^2$) is only 4%, which lead to the inability of distinguishing ^{185}Re from ^{187}Re in the broad spectra and thus

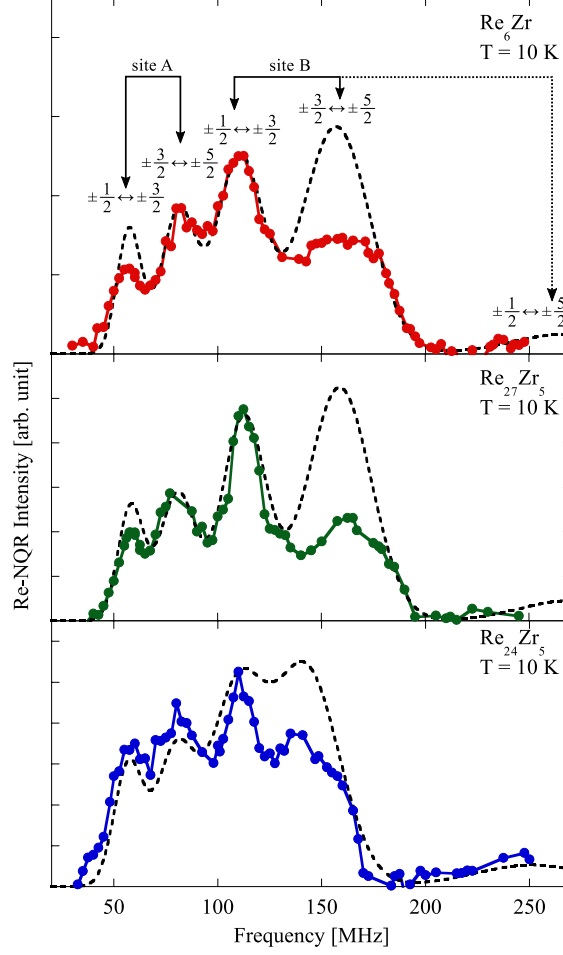


FIG. 3. $^{185/187}\text{Re}$ -NQR spectrum of Re_6Zr , $\text{Re}_{27}\text{Zr}_5$ and $\text{Re}_{24}\text{Zr}_5$ measured at $T = 10$ K. Dotted curves are the theoretical simulations (see text).

only four peaks were observed. As can be seen in Fig. 3, only the uppermost peak varies upon changing the Re-Zr composition ratio. By a theoretical simulation (see below), we assigned the lower two peaks to site A and the upper two peaks to site B. At the moment, it is unclear site A (B) corresponds to which Re site in the crystal structure. The Hamiltonian for the quadrupole interaction is,

$$\mathcal{H} = \frac{\nu_Q}{6} \left\{ (3I^2 - \vec{I}^2) + \frac{\eta}{2} (I_+^2 + I_-^2) \right\}. \quad (1)$$

Here ν_Q and η are defined as

$$\nu_Q \equiv \nu_z = \frac{3}{2I(2I-1)\hbar} e^2 Q \frac{\partial^2 V}{\partial z^2} \quad (2)$$

$$\eta = \frac{|\nu_x - \nu_y|}{\nu_z}, \quad (3)$$

with $\frac{\partial^2 V}{\partial \alpha^2}(\alpha = x, y, z)$ being the electric field gradient at the position of the nucleus. In the simulations, a Gaussian function $\exp\{-(f/2\delta)^2\}$ is convoluted, where f is the frequency and δ is related to the full width at half maximum ($FWHM$) of the transition line as $FWHM = 2\delta\sqrt{2\ln(2)}$. The ν_Q and η were treated as parameters. The intensity ratio of each peak depends on η . With the parameters listed in Table 1, we are able to reproduce the experimental results as seen in Fig. 3. We note that ν_Q or the $FWHM$ is proportional to Q , so the value for ^{185}Re ($Q = 2.7 \times 10^{-24} \text{ cm}^2$) is 1.04 times the value for ^{187}Re ($Q = 2.6 \times 10^{-24} \text{ cm}^2$). The intensity for the uppermost peak does not agree with the simulation, probably due to a worse quality factor of the coil in this frequency range. In the case of large η , signal from the forbidden transitions ($\pm 1/2 \leftrightarrow \pm 5/2$) is expected. Indeed, we detected such signals in the frequency range above 200 MHz as seen in Fig. 3.

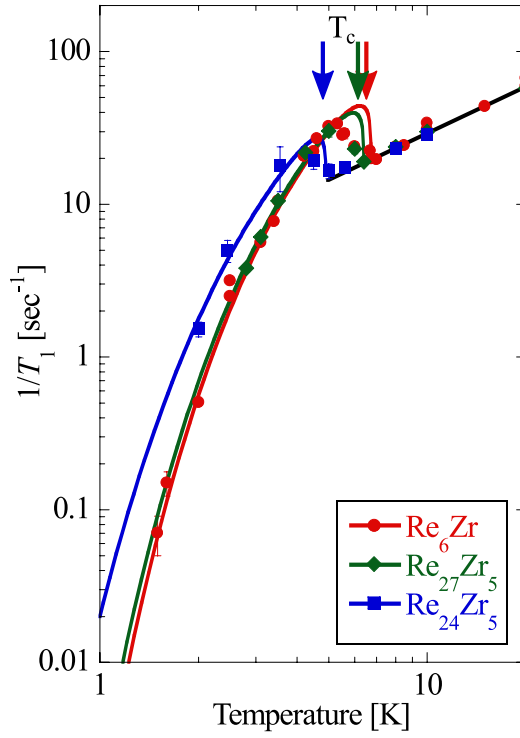


FIG. 4. (color online) Temperature dependence of the spin-lattice relaxation rate $1/T_1$ measured by NQR. The straight line above T_c represents the $T_1 T = \text{const}$ relation. The solid curve below T_c is a calculation assuming the s -wave gap function (see text).

Figure 4 shows the temperature dependence of $1/T_1$ of $^{185/187}\text{Re}$ -NQR, which was measured at the $1\nu_Q$ ($\pm 1/2 \leftrightarrow \pm 3/2$) transition of the site B. The nuclear magnetization decay

curve for each compound is well fitted to the theoretical formula for different η^{23} ,

$$\text{Re}_6\text{Zr} : \frac{M_0 - M(t)}{M_0} = 0.163 \exp\left(-\frac{3.00t}{T_1}\right) + 0.837 \exp\left(-\frac{8.52t}{T_1}\right) \quad (4)$$

$$\text{Re}_{27}\text{Zr}_5 : \frac{M_0 - M(t)}{M_0} = 0.170 \exp\left(-\frac{3.00t}{T_1}\right) + 0.830 \exp\left(-\frac{8.42t}{T_1}\right) \quad (5)$$

$$\text{Re}_{24}\text{Zr}_5 : \frac{M_0 - M(t)}{M_0} = 0.187 \exp\left(-\frac{3.00t}{T_1}\right) + 0.813 \exp\left(-\frac{8.23t}{T_1}\right) \quad (6)$$

where M_0 is the nuclear magnetization in the thermal equilibrium and $M(t)$ is the nuclear magnetization at a time t after the saturating pulse. We have confirmed that T_1 measured at the $\pm 3/2 \leftrightarrow \pm 5/2$ transition gives the same value. The recovery curve can be fitted with a single T_1 component below and above T_c , which indicates that macroscopic phase separation in the sample is small. As seen in the figure, $1/T_1$ varies in proportion to the temperature (T) above T_c for all samples, as expected for conventional metals, indicating no electron-electron interaction. Below T_c , $1/T_1$ shows a coherence peak (Hebel-Slichter peak) expected for an s -wave superconducting state. The $1/T_{1S}$ in the superconducting state is expressed as

$$\begin{aligned} \frac{T_{1N}}{T_{1S}} = \frac{2}{k_B T} \int \left(1 + \frac{\Delta^2}{EE'}\right) N_S(E) N_S(E') \\ \times f(E) [1 - f(E')] \delta(E - E') dE dE', \end{aligned} \quad (7)$$

where $1/T_{1N}$ is the relaxation rate in the normal state, $N_S(E)$ is the superconducting density of states (DOS), $f(E)$ is the Fermi distribution function and $C = 1 + \frac{\Delta^2}{EE'}$ is the coherence factor. To perform the calculation of eq. (6), we follow Hebel to convolute $N_S(E)$ with a broadening function $B(E)^{24}$, which is approximated by a rectangular function centered at E with a height of $1/2\delta$. The solid curve below T_c shown in Fig. 4 is a calculation with $2\Delta = 3.58k_B T_c$, $b \equiv \delta/\Delta(0) = 0.030$ for Re_6Zr , $2\Delta = 3.55k_B T_c$, $b = 0.058$ for $\text{Re}_{27}\text{Zr}_5$, and $2\Delta = 3.51k_B T_c$, $b = 0.107$ for $\text{Re}_{24}\text{Zr}_5$. The curve fits the experimental data reasonably well. The parameter 2Δ is close to the BCS value of $3.53k_B T_c$. This result indicates an isotropic superconducting gap in these compounds. A similar conclusion was drawn by a recent London penetration depth measurement for $\text{Re}_6\text{Zr}^{25}$.

Our result is inconsistent with a time reversal symmetry broken superconducting state such as $d + id$ or $p + ip$ where the coherence peak will be absent. We note that inconsistent results from different probes have been reported in LaNiC_2 , $\text{PrPt}_4\text{Ge}_{12}$, and the locally non-centrosymmetric superconductor SrPtAs that has an inversion center in whole unit cell but not within a single layer. In these samples, time reversal symmetry breaking was

suggested by μSR ^{1,19,26}, but an s -wave superconductivity was confirmed by NQR/NMR measurements^{27–29}. In these materials, breaking of time reversal symmetry has not been observed except for μSR .

IV. SUMMARY

In summary, we have performed the $^{185/187}\text{Re}$ -NQR measurements on the non-centrosymmetric superconductors Re_6Zr , $\text{Re}_{27}\text{Zr}_5$, and $\text{Re}_{24}\text{Zr}_5$. The T -linear behavior of the nuclear spin-lattice relaxation rate $1/T_1$ above T_c indicates the absence of spin correlations. The $1/T_1$ shows a Hebel-Slichter peak just below T_c and decreases exponentially at low temperatures for all samples, which suggests that the α -Mn type Re-Zr system is in an s -wave fully-gapped superconducting state, which is inconsistent with a time reversal symmetry breaking state such as $d + id$ or $p + ip$.

ACKNOWLEDGMENTS

This work was supported by Research Grants, No. 15H05852 (Innovative Areas “Topological Materials Science”) from MEXT and No. 16H04016 from JSPS.

-
- ¹ A. D. Hillier, J. Quintanilla, and R. Cywinski, Phys. Rev. Lett. **102**, 117007 (2009).
 - ² K. Matano, M. Kriener, K. Segawa, Y. Ando, and G.-q. Zheng, Nat. Phys. , **12**, 852-854 (2016).
 - ³ L. P. Gor’kov and E. I. Rashba, Phys. Rev. Lett. **87**, 037004 (2001).
 - ⁴ P. A. Frigeri, D. F. Agterberg, A. Koga, and M. Sigrist, Phys. Rev. Lett. **92**, 097001 (2004).
 - ⁵ P. A. Frigeri, D. F. Agterberg, and M. Sigrist, New Journal of Physics **6**, 115 (2004).
 - ⁶ M. Nishiyama, Y. Inada, and G.-q. Zheng, Phys. Rev. B **71**, 220505 (2005).
 - ⁷ M. Nishiyama, Y. Inada, and G.-q. Zheng, Phys. Rev. Lett. **98**, 047002 (2007).
 - ⁸ H. Q. Yuan, D. F. Agterberg, N. Hayashi, P. Badica, D. Vandervelde, K. Togano, M. Sigrist, and M. B. Salamon, Phys. Rev. Lett. **97**, 017006 (2006).
 - ⁹ S. Harada, J. J. Zhou, Y. G. Yao, Y. Inada, and G.-q. Zheng, Phys. Rev. B **86**, 220502 (2012).
 - ¹⁰ T. Klimczuk, Q. Xu, E. Morosan, J. D. Thompson, H. W. Zandbergen, and R. J. Cava, Phys. Rev. B **74**, 220502 (2006).

- ¹¹ B. Joshi, A. Thamizhavel, and S. Ramakrishnan, Phys. Rev. B **84**, 064518 (2011).
- ¹² Y. Okamoto, T. Inohara, Y. Yamakawa, A. Yamakage, and K. Takenaka, J. Phys. Soc. Jpn. **85**, 013704 (2016).
- ¹³ K. Tahara, Z. Li, H. X. Yang, J. L. Luo, S. Kawasaki, and G.-q. Zheng, Phys. Rev. B **80**, 060503 (2009).
- ¹⁴ K. Matano, S. Maeda, H. Sawaoka, Y. Muro, T. Takabatake, B. Joshi, S. Ramakrishnan, K. Kawashima, J. Akimitsu, and G.-q. Zheng, J. Phys. Soc. Jpn. **82**, 084711 (2013).
- ¹⁵ B. Matthias, J. Phys. Chem. Solids **19**, 130 (1961).
- ¹⁶ R. P. Singh, A. D. Hillier, B. Mazidian, J. Quintanilla, J. F. Annett, D. M. Paul, G. Balakrishnan, and M. R. Lees, Phys. Rev. Lett. **112**, 107002 (2014).
- ¹⁷ D. Hobbs, J. Hafner, and D. Spišák, Phys. Rev. B **68**, 014407 (2003).
- ¹⁸ A. P. Mackenzie and Y. Maeno, Rev. Mod. Phys. **75**, 657 (2003).
- ¹⁹ P. K. Biswas, H. Luetkens, T. Neupert, T. Stürzer, C. Baines, G. Pascua, A. P. Schnyder, M. H. Fischer, J. Goryo, M. R. Lees, H. Maeter, F. Brückner, H.-H. Klauss, M. Nicklas, P. J. Baker, A. D. Hillier, M. Sigrist, A. Amato, and D. Johrendt, Phys. Rev. B **87**, 180503 (2013).
- ²⁰ J. Chen, L. Jiao, J. L. Zhang, Y. Chen, L. Yang, M. Nicklas, F. Steglich, and H. Q. Yuan, Phys. Rev. B **88**, 144510 (2013).
- ²¹ E. M. Savitskii, M. A. Tylkina, and I. A. Tsyganova, The Soviet Journal of Atomic Energy **7**, 724 (1961).
- ²² J.-M. Joubert and M. Phejar, Progress in Materials Science **54**, 945 (2009).
- ²³ J. Chepin and J. H. Ross Jr., J. Phys. Condens. Matter **3**, 8103 (1991).
- ²⁴ L. C. Hebel, Phys. Rev. **116**, 79 (1959).
- ²⁵ M. A. Khan, A. B. Karki, J. C. Prestigiacomo, T. Samanta, D. Browne, S. Stadler, I. Vekhter, P. W. Adams, A. Pandey, R. Prozorov, S. Teknowijoyo, K. Cho, D. E. Graf, and D. P. Young, arXiv:1603.07297 (2016).
- ²⁶ A. Maisuradze, W. Schnelle, R. Khasanov, R. Gumeniuk, M. Nicklas, H. Rosner, A. Leithe-Jasper, Y. Grin, A. Amato, and P. Thalmeier, Phys. Rev. B **82**, 024524 (2010).
- ²⁷ Y. Iwamoto, Y. Iwasaki, K. Ueda, and T. Kohara, Phys. Lett. A **250**, 439 (1998).
- ²⁸ F. Kanetake, H. Mukuda, Y. Kitaoka, K. ichi Magishi, H. Sugawara, K. M. Itoh, and E. E. Haller, J. Phys. Soc. Jpn. **79**, 063702 (2010).

- ²⁹ K. Matano, K. Arima, S. Maeda, Y. Nishikubo, K. Kudo, M. Nohara, and G.-q. Zheng, Phys. Rev. B **89**, 140504 (2014).